Novel Method for Noncontact Measurement of Particle Temperatures

B. M. Wagenaar, R. Meijer, J. A. M. Kuipers, and W. P. M. van Swaaij
Dept. of Chemical Engineering, Twente University of Technology, 7500 AE Enschede, The Netherlands

A nonintrusive temperature measurement technique is developed for noncontact measurement of the temperature of single particles with >200 μm dia. It is based on the temperature dependence of the fluorescence spectrum resulting from irradiation of a certain phosphor mixture with UV light by applying a mixture of two phosphors with fluorescence colors (blue and green) and a color shift from green to blue (with temperature increase from 20 to 280°C). An experimental setup is described for temperature measurement of particles based on the fluorescence color, together with the calibration of this system. The fluoroptic technique is applied to measure the temperature decrease of hot particles flowing down a cold chute. The measurements agree very well with thermocouple measurements. This novel technique can be applied to nonintrusive measurement of particle temperatures in (dense) multiparticle systems as encountered in packed and fluidized beds.

Measurement of Heat Transfer to Particulate Phase

If two positions on a streamline of a particle flow are defined, the heat transfer to the particles equals the ratio of particle thermal energy difference and elapsed particle traveling time between the two points. In systems in which the particle thermal energy content depends only on temperature, the determination of the heat-transfer coefficient can be based on temperature measurements. A number of conventional temperature measurement techniques are available such as direct temperature measurement with thermocouples (Brewster and Seader, 1984), particle collectors (Boothroyd and Hague, 1970; Johnstone et al., 1941), two-color pyrometers (Jorgensen and Zuiderwyk, 1985) and techniques employing the change in magnetic permeability of ferrites (Turton et al., 1989) and techniques involving liquid crystals (Yianneskis, 1986), drying of solids (Debrand, 1974; Vandenschuren and Delvosalle, 1980) and sublimation of solids (Vítovec, 1975). The novel temperature measurement technique described in this article uses the temperature-dependent change of quantum yield of phosphors.

Phosphors are materials capable of emitting visible radiation when subjected to ultraviolet radiation. The quantum efficiency of a phosphor is defined as the ratio of the number of quanta emitted by the phosphor to the number absorbed by the phosphor. The quantum efficiency of some phosphors is temperature-dependent, presenting a possibility of determining the temperature of phosphors by measuring their quantum yield. If a light source is used with a constant UV power output, the temperature of the phosphor depends solely on the intensity of the visible light emitted by the phosphor. This principle forms the bases of the noncontact temperature measurement technique for moving particles in the present work. Thermometers using this technique have been used in wafer temperature control (Egerton et al., 1982).

Advantages of the fluoroptic technique include its capability of measuring the temperature of rapidly moving dispersed powder flows. The technique is also applicable for measurement of rapidly changing temperatures. Disadvantages of the fluoroptic technique in its present state are its limited temperature range (from 100 to 280°C), although this does not constitute a serious limitation in case the convective gas-to-particle heat-transfer coefficient has to be determined since this quantity varies slowly with temperature.

Description of Fluorescence at Atomic Level

The noncontact temperature measurement technique for moving phosphor particles used in this work is based on the temperature-dependent fluorescent spectrum of phosphors. The temperature dependence of the fluorescent spectrum of phosphors can be explained with theories describing the atomic processes of absorption and emission of radiation by the phosphors.

Phosphors are materials capable of emitting visible radiation when subjected to ultraviolet radiation. The quantum efficiency of a phosphor is defined as the ratio of the number of

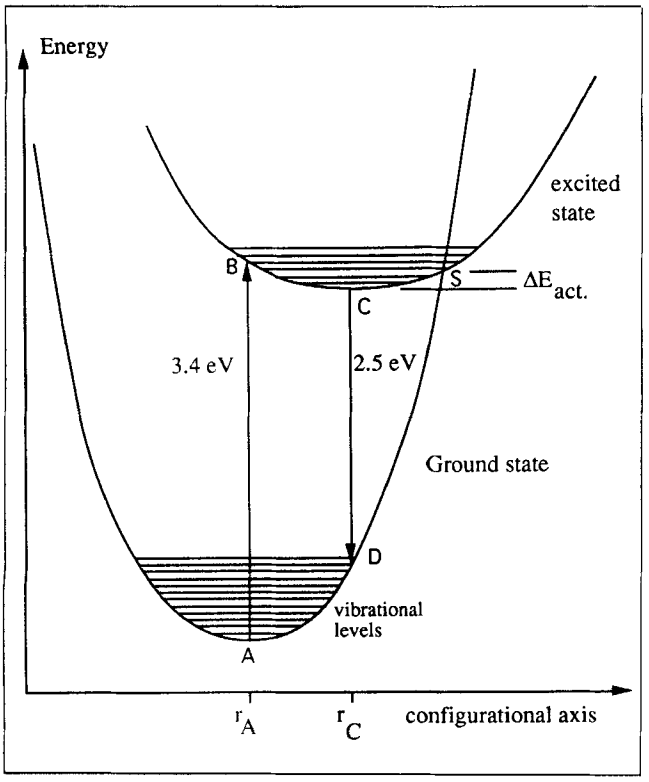

Figure 1. Energy of valence electrons of the luminescent center vs. configuration coordinate.

quanta emitted by the phosphor to the number of quanta absorbed by the phosphor. Phosphors of technical interest have quantum efficiencies of 70 to 90% as reported by Blasse (1970) and Karstens and Kobs (1980).

The fluorescence phenomena of a luminescent center can be explained in terms of an energy vs. configuration-coordinate diagram, as presented in Figure 1. The horizontal axis refers to the mean distance between the luminescent center and the surrounding ions. The vertical axis refers to the energy of the valence electrons of the luminescent center. Without any excitation the luminescent centers of the phosphor remain in their ground state equilibrium coordinate given by point A. Excitation from the ground state to the excited state can occur if the luminescent center absorbs an energy quantum of 3.4 eV (365 nm) after which the center moves to point B. The optical transition between the ground state and the excited state is restricted by the Franck-Condon principle (Blasse, 1970), which states that the electronic energy absorption is some orders faster compared to the time required to move the nucleus to its new position, resulting in vertical jumps in Figure 1. The system moves from B to the equilibrium coordinate C of the excited state by vibrational transitions. The vibration quantum is about 1/50–1/100 of the energy to be disposed of (Kröger, 1948). From this state the luminescent center may return to the ground state in two ways. The first route is the emission of a photon by the luminescent center of 2.5 eV (500 nm). This mode of returning to the ground state is called fluorescence. The second route occurs if the system moves to point S (the intersection of the excited and the ground state) provided that the activation energy ΔE is available. From the

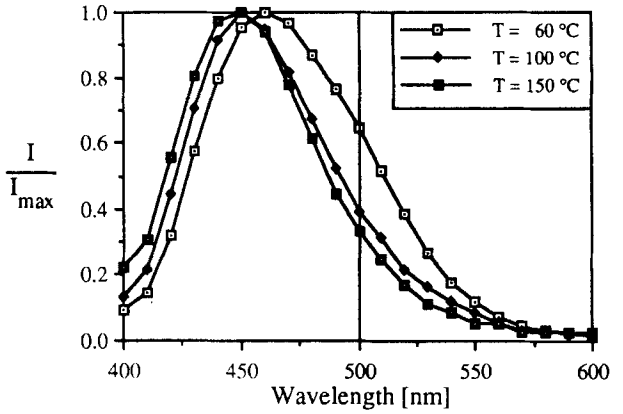

Figure 2. Fluorescence spectrum as function of temperature.

intersection point S the system relaxes to its equilibrium ground state without emitting visible radiation, but releasing only heat dispersed in the mother lattice. At higher temperatures, the activation energy ΔE can be more easily provided and the radiationless transition becomes more likely, a phenomenon termed the thermal quenching of a phosphor.

The commercial available phosphors show only a minor color change upon heating. A better way to obtain a significant color change would be the use of a phosphor mixture consisting of a phosphor showing thermal quenching at a relative low temperature, whereas the fluorescence intensity of the second phosphor is not affected at elevated temperatures. The fluorescence spectrum of such a phosphor mixture is given in Figure 2.

This mixture consists of: phosphor $BaMgAl_{10}O_{17}$:Eu (1.0 g, blue); phosphor $Sr_4Al_{14}O_{25}$:Eu (1.0 g, green). The thermal quenching of the green emitting phosphor with an intensity maximum at 488 nm occurs at temperatures above 100°C. At 250°C the spectrum is dominated by the blue phosphor with an intensity peak at 447 nm.

The fluoroptic measurement method is basically a two color measurement method since the temperature is related to the intensity ratio of two fluorescent colors, advantageous in conjunction with the elimination of several disturbing influences. If, for example, the amount of detected fluorescent material increases, the fluorescence intensity as detected by a single color method will increase correspondingly, but the detected intensity ratio of the two color method remains the same.

Experimental Setup

The fluoroptic setup consists of a light source that generates the primary UV radiation. This primary UV radiation possesses a broad spectrum from which the desired wavelength domain is selected with aid of a proper UV filter. A quartz fiber cable guides the filtered UV radiation (2 W) to the measuring spot, Figure 3. Fluorescent particles are traveling through this spot and upon illumination with UV radiation the particles emit visible radiation (observable as a color change) corresponding in a unique way to the particle temperature. The visible radiation emitted by the particles is collected with a glass fiber cable and guided to optical filters that separate the color signal into a blue and green component. The resulting optical signal

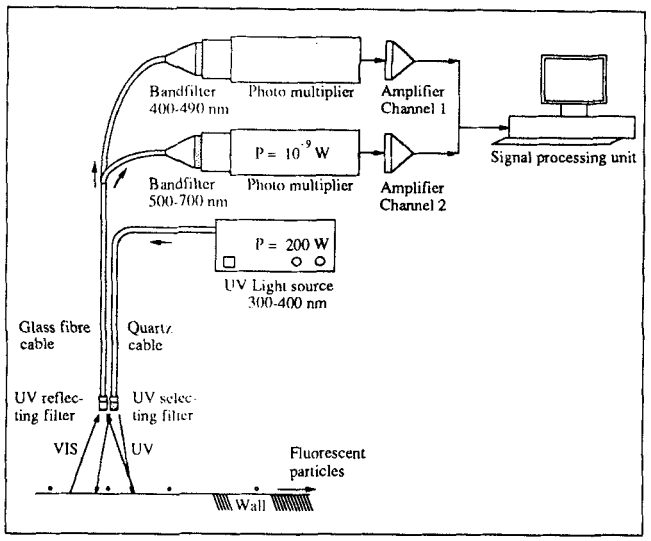

Figure 3. Fluoroptic measurement setup.

is then transformed into an electrical signal with use of photomultipliers that simultaneously amplify the electrical signal. Finally, the electrical signal is sent to a date acquisition unit for further processing. The elements of this setup are presented in Figure 3.

The cross section of the illuminated spot is approximately 1 cm which corresponds in the case of 100-μm particles to a ratio of particle to spot cross-sectional area of about 10^{-4}. Consequently, if the background wall acts as a perfect reflector, the photons captured by the signal transmitting glass fiber consist of 10^{-4} part VIS photons and 1 part UV photons. Only the visible photons carry the temperature information; therefore, the UV photons have to be removed before they reach the photon detector. In this case a blockage factor of 10^{-6} for the UV photons results in a UV signal after blocking, which still amounts to 1% of the total visible signal. The assumption of a perfect reflecting background is rather severe, but a reactor wall reflectivity less than 1% is difficult to achieve in engineering applications. In the present study the cross-sectional dia. of the illuminated spot equals 10 mm whereas the maximum particle velocity is about 10 $m \cdot s^{-1}$, which implies that the temperature of a particle has to be measured in less than 1 ms.

It should be mentioned that the maximum heating due to illumination of the particles can be calculated on the basis of the assumption of complete absorption of the UV radiation and subsequent conversion of this energy influx into heat. Calculations showed that the smallest particles only experience a temperature rise of about 0.1 K due to this phenomenon.

Every light source of given intensity emits an average amount of photons per unit time. Since the actual event of a photon emission occurs randomly, the process of photon emission can be described by Poisson statistics (Robben, 1971). If the light source produces I photons per second and the photomultiplier output is measured over a period of time t, the signal (S) is:

$$S = I \cdot t \tag{1}$$

Due to the corpuscular character of light an uncertainty in the measurement of signal S results, which can be described by the standard deviation of signal S. The standard deviation or the associated noise (N) in signal S is equal to:

$$N = \sqrt{(I \cdot t)} \tag{2}$$

The noise-to-signal ratio is given by:

$$\frac{N}{S} = \frac{1}{\sqrt{S}} \tag{3}$$

and can be reduced by increasing the amount of detected photons (S).

Hardware Components

Figure 3 shows all the essential components of the fluoroptic measurement system.

Arc lamp

A high-pressure, direct-current, mercury arc lamp (type Ushio USH-205S) has been used with an electrical dissipation of 200 W in the light bulb.

Quartz light guide

A quartz cable has been used as the light guide, because this cable type enables transmission of ultraviolet light with an overall efficiency of 30%. Additionally, it can withstand temperatures in excess of 250°C for a long operating time.

Schott DUG 11 filter

This filter has been positioned at the end of the quartz cable and transmits the ultraviolet light with a wavelength in the 300–400 nm range. In the remaining part of the optical system a monochromatic blockage factor of 10^6 is achieved for ultraviolet light in the aforementioned wavelength range.

Balzer UV reflecting filter

All optical components between fluorescent particle and UV blocker have been selected with great care to avoid self-fluorescence of these components. Self-fluorescence represents (undesired) conversion of ultraviolet radiation into visible radiation and is a property of almost every optical component. In order to avoid any self-fluorescence of the optical components, a Balzer UV reflecting filter has been positioned immediately before the location where the light emitted by the fluorescent particles enters the light guide. This filter containing a coating on one side of a glass substrate reflects more than 99% of the UV radiation with wavelengths smaller than 380 nm. This filter can withstand temperatures up to 400°C for a long operating time.

Glass fiber light guide

A low cost optical fiber of Dolan and Jenner protected from UV radiation with aid of the Balzer filter serves as the light guide. The light transmitting cable receives visible light from particles in the measuring spot and guides the visible light to the color separating filters.

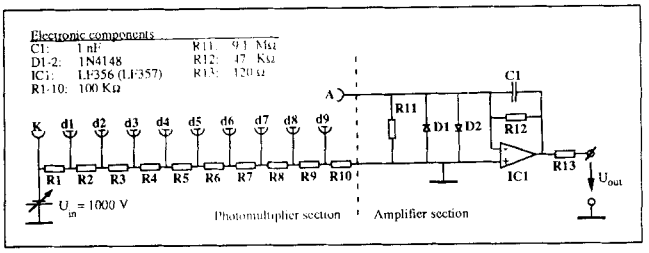

Figure 4. Electronic amplification circuit consisting of photomultiplier section and amplifier section.

Microscope oculars

Microscope oculars provide an efficient way to create a parallel light bundle in which optical filters can be placed. After passing the bandfilters the light bundle is projected on the light sensitive cathode area of the photomultiplier.

Bandfilters

Two bandfilters were applied to separate the light emitted by the particles into two colors: a Schott BSF Magenta bandfilter is used to select a wavelength interval of 400–490 nm (blue light transmission); a Schott KV500 bandfilter is used to select a wavelength interval of 500–700 nm (green light transmission).

Photomultipliers

Two Hamamatsu R928 photomultipliers were used which possess an amplification factor of 10^7 between the cathode current and the anode current at 1,000 V acceleration voltage. A photon flow of $2 \cdot 10^{-10}$ W at 500-nm wavelength generates at 1,000 V acceleration voltage the maximum allowable anode current of 100 μA.

Electronic amplification circuit

The electronic amplification circuit presented in Figure 4 shows the photomultiplier and amplifier section. The resistance network R1–R10 provides equal potential differences between the dynodes of the photomultiplier. The single event of a photon detection at the cathode (K) produces a photomultiplier output current at the anode (A) with peaks of 1 ns duration. These peaks are damped in the amplifier section by condensator C1. The RC time τ_{RC} = R12*C1 equals 47 μs, and can be adjusted by changing the condensator capacity C1, but should be kept significantly smaller in comparison to the time scale of a particle passage, which is approximately 1 ms. This RC-time limits the response rate of the electronic system.

Signal processing

An IBM compatible microcomputer was used to facilitate the data acquisition and the data analysis. Conversion of the amplified output signal into digital data was obtained via a 12-bit AD-converter (Analog Devices, model RTI 815A) connected into an expansion slot of the microcomputer. High frequency sampling (maximum rate 31 kHz) was achieved by storing the data in the computer memory buffer with direct access.

Powder Preparation

The particles which were used as fluorescent temperature indicators consist of the following three components:

- A barium magnesium aluminate phosphor (BAM) of chemical composition $BaMgAl_{10}O_{17}$:Eu. The double dot notation indicates that the mother crystal lattice of $BaMgAl_{10}O_{17}$ is doped with the rare earth element Europium. The corresponding phosphor particles have a diameter of 3.4 μm and an intrinsic particle density of 3,800 $kg \cdot m^{-3}$. This phosphor (Philips type U716) emits blue light upon excitation with ultraviolet light and possesses a peak spectral response at a wavelength of 447 nm.
- A strontium aluminate phosphor (SAE) of chemical composition $Sr_4Al_{14}O_{25}$:Eu. These phosphor particles have a diameter of 6.0 μm and an intrinsic particle density of 3,690 $kg \cdot m^{-3}$. This phosphor (Philips type U724) emits green light upon excitation with ultraviolet light and possesses a peak spectral response at a wavelength of 488 nm.
- A low melting glasseous binding material, that is, lead-mono-silicate $PbO(SiO_2)_{1.03}$, binds the phosphors into its matrix. This material is transparent, grindable and can be used as solid particles up to 553 K.

According to safety data sheets supplied by Philips, the two phosphors mentioned above are harmless with respect to health, although the reader should first take notion of the data sheets before using the BAM and SAE phosphors.

Appropriate amounts of both phosphors were thoroughly mixed with molten Lead-monosilicate. After solidification of the mixture, particles of suitable size (that is, 100–1,000 μm) were obtained by grinding; a presentation of a single particle temperature indicator is given in Figure 5.

The spectrum of a mixture consisting of a BAM and SAE phosphor can be calculated by adding and mass weighing the spectra of the individual phosphors. This procedure can be used if the phosphors only absorb UV radiation and only emit VIS radiation. In other cases an interaction between the two phosphors exits whose magnitude cannot be calculated theoretically. The temperature dependence of the fluorescence spectrum of the phosphor mixture should then be obtained by calibration.

Calibration and Validation of Fluoroptic Method

Calibration

The functional dependency which relates the measured green-to-blue intensity ratio to the particle temperature must be obtained by calibration. Subsequently, the calibration of the fluoroptic measuring system will be described in detail.

A sample of particles was placed on a heated surface with a temperature that could be varied from 20 to 300°C. The surface temperature was measured with a thermocouple. The sample was illuminated continuously which yielded the measured green-to-blue intensity ratio given in Figure 6. As mentioned before, in systems of engineering interest the particles usually move through the illuminated spot which corresponds to nonstationary illumination. To simulate this effect, the UV beam illuminating the particles was chopped by a disk with a narrow slit rotating at an appropriate frequency. The light pulses generated with this technique had a duration of approximately 1 millisecond. The results of these measurements

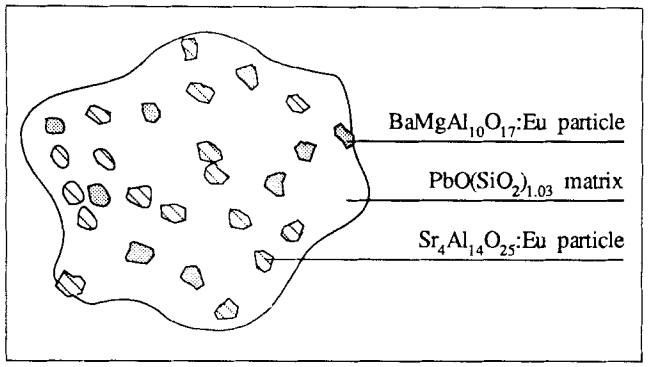

Figure 5. Temperature indicating particle.

are also shown in Figure 6 from which a small dynamical effect is evident. This effect causes a maximum error of 10°C in temperature measurement.

In addition to the dynamical effect from an optical point of view, the dynamical effect from a thermal viewpoint has been investigated. To study the latter dynamical effect, the rate of signal response caused by a very rapid temperature change was recorded when conducting a heating on contact experiment. In this experiment the phosphor mixture was placed upon an aluminum foil of 11 μm thickness, which was subsequently instantaneously brought in contact with a soldering iron of 230°C at the lower side. The rate of change of the measured green-to-blue intensity ratio, shown in Figure 7, indicates a response time of approximately 20 ms. Additional heat-transfer resistances (air gaps) probably exist between the soldering iron and the phosphors but have not been identified. The measured thermal response rate of the phosphors is a conservative estimate.

The reverse dynamical effect (occurring upon cooling) was also studied by contacting the hot aluminum foil instantaneously with cold water at the lower side, and recording the resulting signal change as a function of time. From this experiment again a response time of approximately 20 ms was obtained. Due to other heat-transfer resistances, this response time also constitutes a conservative estimate.

Validation

In addition to the aforementioned experiments, which yielded valuable information with regard to the dynamical behavior

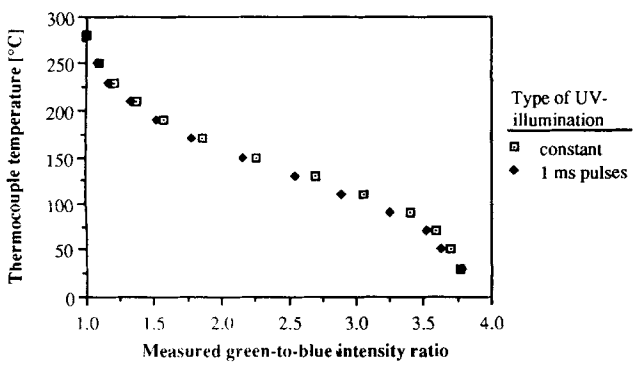

Figure 6. Measured thermocouple temperature vs. measured green-to-blue intensity ratio under various illumination conditions.

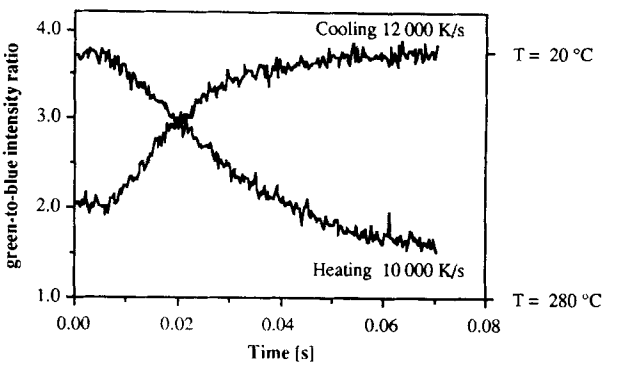

Figure 7. Measured response of the fluoroptic system caused by rapid temperature changes of phosphors.

from both an optical and thermal viewpoint, an additional test was carried out to study the performance of the fluoroptic method. A specially developed thermal conditioned drop tube (0.5 m in length) was used to produce a particle flow of which the temperature at the tube exit was known within 5°C. Fluoroptic measurements at the drop tube exit are presented in Figure 8 as a function of the latter temperature.

As evident from Figure 8, the deviation of the particle temperature from the drop tube temperature is less than 20°C in the temperature range from 100 to 250°C. This deviation is caused by the use of commercial available phosphors, not specifically developed for temperature measurements. It is anticipated that a substantial reduction in the error of the temperature measurement can be obtained by employing more dedicated phosphors. In the present study a measurement error of 20°C was considered to be acceptable.

A final test experiment was performed to establish the independence of the measured green-to-blue intensity ratio with regard to the mass-flow rate of fluorescent particles. An isothermal flow of fluorescent particles with varying mass-flow rate was monitored with the fluoroptic method resulting in a time-dependent signal, as shown in Figure 9. The signal strength of each channel varied between 200 and 1,400 mV, which corresponds to a seven-fold increase in the particle mass-flow rate. However, the measured green-to-blue intensity ratio also

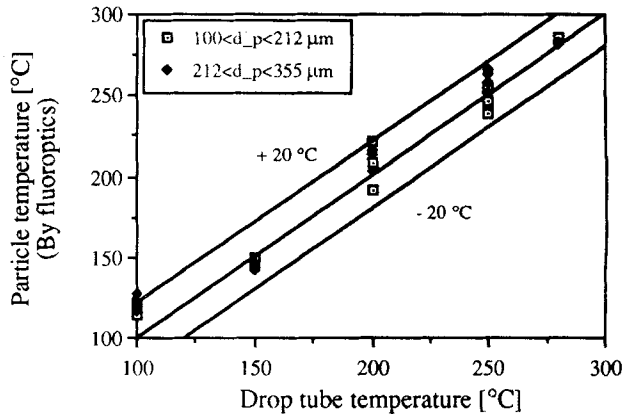

Figure 8. Particle temperature measured with fluoroptic method vs. drop tube temperature at exit.

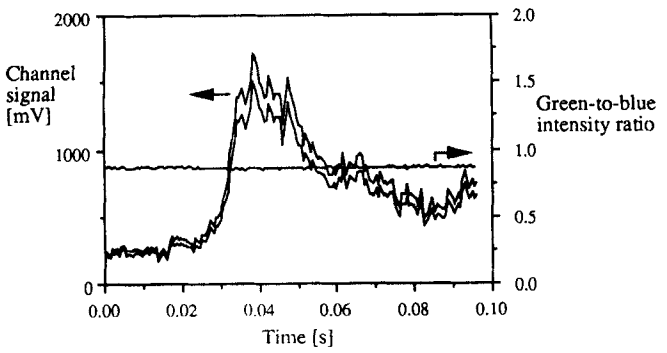

Figure 9. Measured light intensity of each channel and green-to-blue intensity ratio as function of time in cold flow experiment with varying mass-flow rate of fluorescent particles.

given in Figure 9 varied less than 1%. The measured green-to-blue intensity ratio shows no dependence on the mass-flow rate, which constitutes a major advantage of the two color measurement method in comparison with a single color method. In the next section temperature measurements of a dilute particle flow along an inclined chute will be reported.

Temperature Measurement of Particles Flowing Along Inclined Chute

Inclined chutes are encountered in the transport of materials such as coal, shale, metal ores, dry chemicals, and grain. Examples of industrial processes which involve heating or cooling of solids are: the dehydration of calcium sulfate for gypsum production, the cooling of charcoal before packaging, the use of ceramics as heat carrier in a solar energy converter, and the use of lithium oxide in the rotating cone granular blanket fusion reactor (Pitts and Walton, 1985). The geometry of the inclined chute offers the advantage that measurement of the local temperature and velocity of a dilute particle flow can be performed easily.

A representation of the experimental setup is shown in Figure 10. This setup has been used for the measurement of the local

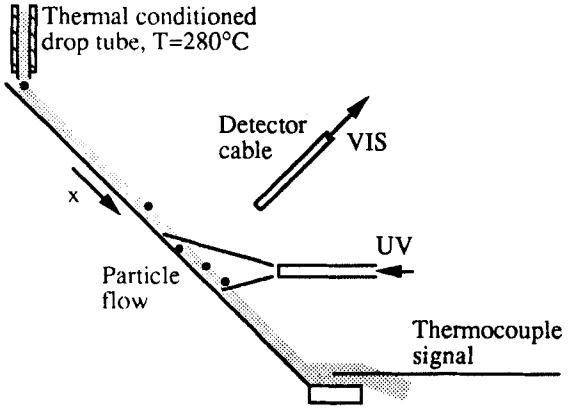

Figure 10. Experimental chute setup for temperature measurements along inclined chute using the fluoroptic method.

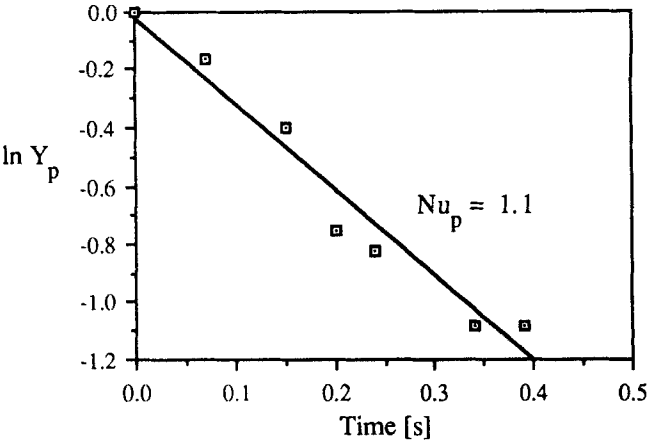

Figure 11. Dimensionless particle temperature Y_p, defined by Eq. 4 as function of the particle contact time.

Inclination angle of the chute equals 43°; glass beads used had a particle diameter of approximately 170 μm, and an intrinsic density of 2,450 kg·m^{-3}.

particle temperature in dilute particle flows along an inclined chute using the fluoroptic temperature measuring method. A thermal conditioned drop tube (see the validation experiments) was used to feed particles with a well-defined temperature at the top of the chute. A piece of thermal insulating material was placed at the end of the chute to concentrate the particle flow. Thermocouples placed in this dense particle flow produced a temperature signal which corresponded within 2°C with measurements using a two-color pyrometer that viewed the thermocouple measurement area.

The equations that describe the heating or cooling of free bodies involves the definition of a dimensionless thermal driving force Y_p:

$$Y_p = \frac{T_p - T_{\text{gas phase}}}{T_{p,\text{feed}} - T_{\text{gas phase}}} \tag{4}$$

The temperature of the gas phase at sufficient distance from the particles equals room temperature (20°C). If the particle internal heat-transfer resistance can be neglected, which is allowable for particle Biot numbers smaller than 0.2, the change of particle temperature with time is given by Eq. 5:

$$Y = e^{-6\alpha_p t/\rho_p C_p d_p} \tag{5}$$

where $\rho_p C_p$ represents the volumetric heat capacity of fluorescent particles. Equation 5 can be used to calculate the particle heat-transfer coefficient α_p from the measured variation of the dimensionless particle temperature Y_p with time t.

For reference purposes local thermocouple measurements were carried out prior to the measurement with the fluoroptic method. Results of these measurements are shown in Figure 11.

The time basis of Figure 11 was obtained by measuring the local particle velocity at different positions along the chute by a photographic technique described in more detail elsewhere (Wagenaar, 1994). Local particle temperature measurements obtained with the fluoroptic method are presented in Figure

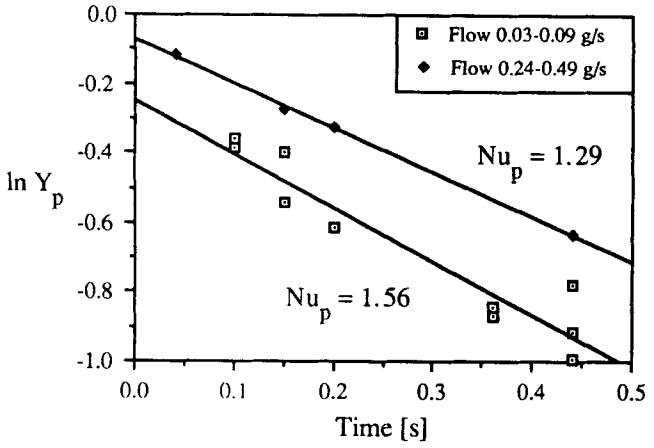

Figure 12. Dimensionless particle temperature Y_p, defined by Eq. 4, as function of time.

Inclination angle of the chute equals 40°; phosphor particles used had a particle diameter of approximately 280 μm, and an intrinsic density of 6,200 kg·m^{-3}.

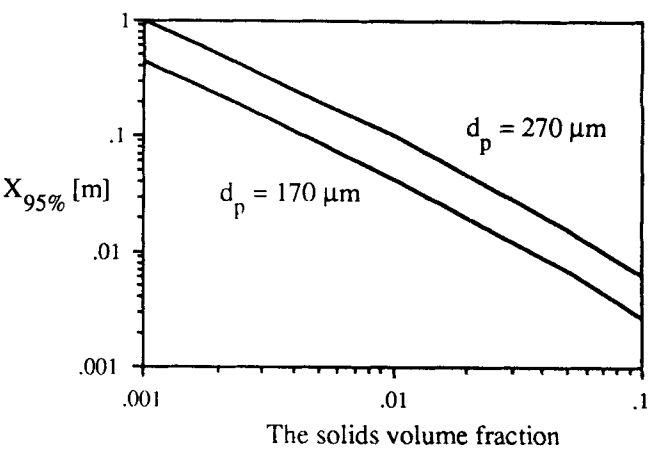

Figure 13. Length $X_{95\%}$ along a streamline where gas-phase velocity increases from 0 to 95% of particle velocity.

12, and give a particle Nusselt number ($Nu_p = 1.29$) which agrees reasonably with the particle Nusselt number obtained with the thermocouple measurements ($Nu_p = 1.1$).

The observed Nusselt numbers for the present dilute particle flow are somewhat smaller compared with Nusselt numbers predicted on basis of the correlation obtained by Ranz and Marshall (1952):

$$Nu_p = 2 + 0.6\, Re_p^{0.5} Pr^{0.33} \tag{6}$$

Where the particle Reynolds number is defined as:

$$Re_p = \frac{\rho_f |u_x - v_p| d_p}{\eta_f} \tag{7}$$

The measurements presented in Figure 12 correspond to two different mass-flow rates. An increase in the mass-flow rate, or equivalently the particle volumetric concentration, results in a decrease of the particle Nusselt number. The magnitude of the Nusselt numbers observed in the present study can be explained through the mutual interaction between the particle phase and gas phase. The mutual interaction between the gas phase and particle phase is twofold, and occurs through momentum coupling and thermal coupling. Both types of interaction will be discussed briefly in the subsequent analysis.

Momentum coupling

The effect of this phenomenon can be estimated by considering the reduced gas-phase momentum equation for steady one-dimensional gas-solid two-phase flow. (See Kuipers, 1990). If the coordinate direction parallel to the chute surface corresponds to the x-direction, the x-component of the reduced gas phase momentum balance is given by:

$$\frac{\partial}{\partial x} \epsilon \rho_f u_x^2 = -\beta (u_x - v_p) \tag{8}$$

In Eq. 8 β represents the interphase momentum exchange between the particle phase and the gas phase and is given by:

$$\beta = \frac{3}{4} \frac{1-\epsilon}{d_p} \rho_f |u - v_p| C_{d,\epsilon=1} f(\epsilon) \tag{9}$$

Where $C_{d,\epsilon=1}$ represents the drag coefficient for a single isolated particle. For particle Reynolds numbers smaller than 10^5 the drag coefficient $C_{d,\epsilon=1} = C_d$ is given by Haider and Levenspiel (1989):

$$C_d = \frac{24}{Re}(1 + 0.14\, Re^{0.653}) + \frac{0.46}{1 + (2{,}700/Re)} \tag{10}$$

In Eq. 9 the function $f(\epsilon)$ accounts for the presence of other particles in the gas phase and corrects the drag force coefficient for single isolated particles and is given by:

$$f(\epsilon) = \epsilon^{-2.65} \tag{11}$$

The particle velocity v_p in Eq. 8 is assumed to be constant and equal to the experimentally determined average value (typically 1 m·s^{-1}). The differential Eq. 8 supplemented with constitutive Eq. 9 and initial condition:

$$u(x=0) = 0 \text{ m·s}^{-1}. \tag{12}$$

can be solved with a simple Runge-Kutta numerical integration procedure yielding u_x as a function of the x-coordinate.

On the basis of the gas-phase velocity profile along the chute length, the length $x_{95\%}$ can be calculated where the gas phase has acquired 95% of the particle velocity. Under the actual experimental conditions the solids volume fraction (1-ϵ) equals 0.002, whereas the chute has a length of 1 m. Figure 13 shows $X_{95\%}$ as a function of the solids volume fraction (1-ϵ). From this figure it can be deduced that significant momentum coupling occurs in the present experimental system. The momentum coupling causes a reduction of the actual velocity difference between the particle and the gas phase. If the Ranz-Marshall

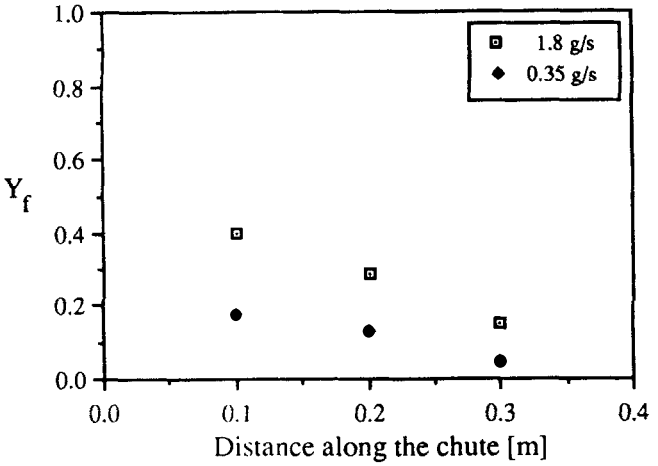

Figure 14. Dimensionless gas-phase temperature defined by Eq. 12 as function of the distance along the inclined chute.

Two different particle feed rates are used (0.35 and 1.8 g/s). Chute length equals 1.0 m; chute width equals 0.05 m.

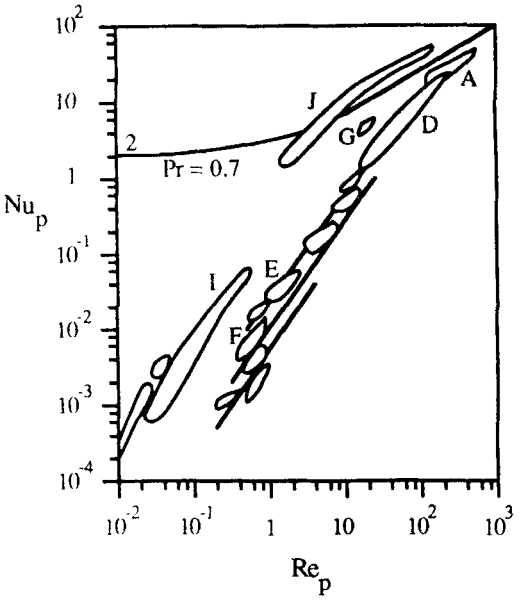

Figure 15. Particle Nusselt number as function of the particle Reynolds number.

Kunii and Levenspiel (1969).

Eq. 6 is evaluated in the prevailing case (that is, $Re \approx 0$), the Nusselt number will tend to the limiting value of 2.

Thermal coupling

Thermal coupling occurs if the heat exchange between the gas phase and the particles results in a change in the local bulk temperature of the gas phase. For measurement of the gas-phase temperature between the particles, a thermocouple was positioned in the dilute particle flow in downstream position and was effectively shielded from the particles. Results of these measurements are presented in Figure 14 and show a thermal coupling between the gas and particulate phase. In this case hot particles (250°C) flowed down an inclined chute at ambient temperature (20°C). The dimensionless gas-phase temperature used in Figure 14 is defined as:

$$Y_f = \frac{T_f - T_{\text{ambient}}}{T_{p,\text{feed}} - T_{\text{ambient}}} \tag{13}$$

The ambient gas-phase temperature is equal to 20°C (room temperature). The heated gas phase surrounding the particles reduces the thermal driving force for heat transfer between the particles and the directly surrounding gas phase.

Due to momentum and thermal coupling, the particle Nusselt number is reduced to values of approximately 1 as can be seen from experimental data shown in Figures 11 and 12. The reduction of the particle Nusselt number is a well-known phenomenon in packed and fluidized beds. Figure 15 contains the results of several experimental studies and shows a drastic reduction of the Nusselt numbers for values of the particle Reynolds number smaller than 10. However, as stressed by Levenspiel et al. (1989), these experimental data depend on theoretical models which not necessarily correspond to physical reality.

Several explanations have been put forward for these phenomena. For instance, Schlünder (1980) proposed a channeling mechanism in which a large fraction of the particles is in equilibrium with their surrounding gas phase and driving force only exists towards a few larger channels through which a large fraction of the gas throughput flows. This mechanism shows some resemblance with the situation on the chute where the particles reduce their local driving force without affecting the ultimate thermal driving force ($T_p - T_{\text{ambient}}$).

This explanation shows the problems that can be encountered to provide a sound descriptive basis for the gas-to-particle heat transfer at low Reynolds and Nusselt numbers. However, it should be stressed that this work was concerned with the development and experimental validation of the fluoroptic technique (temperature measurement of rapidly moving particles). Therefore, the particle temperature has been measured in a very well accessible experimental setup under realistic flow conditions. Temperature measurements performed with thermocouples and the fluoroptic technique proved the validity of the latter.

Conclusion

A novel temperature measurement technique has been developed which permits nonintrusive measurement of the temperature of rapidly moving single particles. The response rate of the novel system has been investigated, both from an optical and a thermal point of view. The fluoroptic method was tested by the following methods:

(1) The optical response speed was measured and proved to be in the order of 1 ms, as shown in Figure 6. The optical response time should always be less than the time required by the particle to travel through the spot to avoid the optical dynamic limitations of the present phosphor system. If higher particle velocities occur, the measuring spot should be enlarged. As mentioned before: particles moving with a velocity of 10 $m \cdot s^{-1}$ will travel through an illuminated spot with a

cross-sectional diameter of 10 mm within 1 ms. The optical response of the phosphors on UV-illumination times less than 1 ms have not yet been tested.

(2) The thermal response rate of the phosphors measured showed that it exceeds 10,000 $K \cdot s^{-1}$, as shown in Figure 7.

(3) An experiment in which the particle temperature was accurately known showed that the temperature of heated particles could be measured in short measuring times that are characteristic of the fluoroptic measurement method, as shown in Figure 8.

All tests revealed a good performance of the phosphors.

It must be stressed that the BAM/SAE phosphor combination used in the present work was not developed specifically for temperature measurements. Application of a phosphor like Dy:YAG, which has been studied by Goss et al. (1989), can broaden the temperature range to 1,000 K which will probably reduce measurement errors. To further develop the fluoroptic measuring technique, every component has to be characterized under dynamic conditions. Therefore, future work will be concerned in duplicating the work of Hilpert (1933) on the heat transfer to wires and cylinders to study all characteristics of the fluoroptic technique in detail in a well-defined experimental environment. (When heated to a plastic state, the glasseous binder material can perfectly be drawn into wires.)

An inclined chute has been used to determine the local particle velocities and temperatures along the chute. This geometry offers the advantage of an easy access. A comparison of Figures 11 and 12 reveals that two independent methods (the thermocouple method and the fluoroptic method) produce similar Nusselt numbers in the order of 1. However, the physical interpretation of the heat transfer from the gas phase to the particles is far from being simple due to the phase coupling effects. These coupling effects include momentum coupling between the particle and gas phase, and thermal coupling between the particle and gas phase; even at a particle volume fraction of 0.002.

The novel technique developed in this work is expected to be applicable to nonintrusive measurement of particle temperatures in:

- Circulating fluidized beds and pneumatic conveyors.
- Drop tube reactors.
- Both gas and liquid fluidized beds.
- Heat-transfer studies involving mixing of two solid phases.

In this case, only one phase should contain fluorescent particles to enable phase selective temperature measurements during the mixing of the two solid phases.

Acknowledgments

We acknowledge M. G. P. Hölscher and M. R. Meijer for their assistance in the experimental work. We also acknowledge the Philips Laboratories for the technical support they gave during the development of the fluoroptic measurement technique.

Notation

C = electrical capacity, F
C_d = drag coefficient
C_p = heat capacity, $J \cdot kg^{-1} \cdot K^{-1}$
d_p = particle diameter, m
I = photon flux, s^{-1}
N = noise, photon
Nu_p = particle Nusselt number ($\alpha d_p / \lambda_f$)
P = power, W
Pr = Prandtl number ($\eta_f C_{p,f} / \lambda_f$)
r = configurational coordinate, m
R = electrical resistance, ohm
Re_p = particle Reynolds number ($\rho_f | u_f - v_p | d_p / \eta_f$)
S = signal, photon
t = time, s
T = temperature, K
u = fluidum velocity, $m \cdot s^{-1}$
U = voltage, V
v = particle velocity, $m \cdot s^{-1}$
x = chute coordinate, m
Y = thermal driving force

Greek letters

α = heat-transfer coefficient, $W \cdot m^{-2} \cdot K^{-1}$
β = volumetric interphase momentum transfer coefficient, $kg \cdot m^{-3} \cdot s^{-1}$
ϵ = porosity, $m^3_{gas} \cdot m^{-3}_{reactor}$
η = viscosity, Pa·s
λ = thermal conductivity, $W \cdot m^{-1} \cdot K^{-1}$
$\lambda_{1,2}$ = wavelength, m
ρ = density, $kg \cdot m^{-3}$

Subscripts

p = particle
f = fluidum

Literature Cited

Bird, R. B., W. E. Stewart, and E. N. Lightfoot, *Transport Phenomena*, Wiley, New York (1960).

Blasse, G., and A. Bril, "Characteristic Luminescence: II. The Efficiency of Phosphors Excited in the Activator," *Philips Tech. Rev.*, **31**, 10 (1970).

Boothroyd, R. G., and H. Haque, "Experimental Investigation of Heat Transfer in the Entrance Region of a Heated Duct Conveying Fine Particles," *Trans. Instn. Chem. Eng.*, **48**, 109 (1970).

Brewster, B. S., and J. D. Seader, "Measuring Temperature in a Flowing Gas-Solids Suspension with a Thermocouple," *AIChE J.*, **30**, 676 (1984).

Debrand, S., "Heat Transfer During a Flash Drying Process," *Ind. Eng. Chem. Proc. Des. Dev.*, **13**, 396 (1974).

Egerton, E. J., A. Nef, W. Millikin, W. Cook, and D. Baril, "Positive Wafer Temperature Control to Increase Dry Etch Throughput and Yield," *Solid State Tech.*, **25**, 84 (1982).

Goss, L. P., A. A. Smith, and M. E. Post, "Surface Thermometry by Laser-Induced Fluorescence," *Rev. Sci. Instrum.*, **60**, 3072 (1989).

Haider, A., and O. Levenspiel, "Drag Coefficient and Terminal Velocity of Spherical and Nonspherical Particles," *Powder Technol.*, **58**, 63 (1989).

Hilpert, R., "Wärmeabgabe von geheizten Drähten und Rohren im Luftstrom," *Forsch. Gebiete Ingenieurw.*, **4**, 215 (1933).

Johnston, H. F., R. L. Pigford, and J. H. Chaplin, "Heat Transfer to Clouds of Falling Particles," *Trans. Am. Inst. Chem. Eng.*, **37**, 95 (1941).

Jorgensen, F. R. A., and M. Zuiderwyk, "Two-Colour Pyrometer Measurement of the Temperature of Individual Combusting Particles," *J. Phys. E: Sci. Instrum.*, **18**, 486 (1985).

Karstens, T., and K. Kobs, "Rhodamine B and Rhodamine 101 as Reference Substances for Fluorescence Quantum Yield Measurements," *J. Phys. Chem.*, **84**, 1871 (1980).

Kröger, F. A., *Some Aspects of the Luminescence of Solids*, Elsevier (1948).

Kuipers, J. A. M., "A Two-Fluid Micro Balance Model of Fluidized Beds," Thesis, University of Twente, The Netherlands (1990).

Kunii, D., and O. Levenspiel, *Fluidization Engineering*, Wiley, New York (1969).

Pitts, J. H., and O. R. Walton, "Flow Characteristics of the Cascade Granular Blanket," *Fusion Technol.*, **8** (1985).

Ranz, W. E., and W. R. Marshall, "Evaporation from Drops: I," *Chem. Eng. Prog.*, **48**, 141 (1952).
Robben, F., "Noise in the Measurement of Light with Photomultipliers," *Appl. Opt.*, **10**, 776 (1971).
Turton, R., T. J. Fitzgerald, and O. Levenspiel, "An Experimental Method to Determine the Heat Transfer Coefficient between Fine Fluidized Particles and Air Via Changes in Magnetic Properties," *Int. J. Heat Mass Transf.*, **32**, 289 (1989).
Vandenschuren, J., and C. Delvosalle, "Particle-to-Particle Heat Transfer in Fluidized Bed Drying," *Chem. Eng. Sci.*, **35**, 1741 (1980).
Vítovec, J., "Heat Transfer Between a Heated Surface and a Fluidized Bed in Sublimation," *Chem. Eng. J.*, **10**, 235 (1975).
Wagenaar, B. M., J. A. M. Kuipers, and W. P. M. van Swaaij, "Particle Dynamics and Gas Phase Hydrodynamics in a Rotating Cone Reactor," *Chem. Eng. Sci.*, submitted (1993).
Yianneskis, M., "Thermal Monitoring by Liquid Crystals," Int. Conf. on Cond. Monitoring, Brighton, England (1986).

Manuscript received Aug. 16, 1993, and revision received Jan. 24, 1994.